AGU PUBLICATIONS

JGR

Journal of Geophysical Research: Solid Earth

RESEARCH ARTICLE

10.1002/2014JB010989

Key Points:
- Velocities from high-resolution seismic data can be used to quantify shallow gas
- Gas volume fraction in the gas-charged Holocene mud is an average 0.046%
- Free gas occurs vertically throughout most of the Holocene mud in the Baltic

Correspondence to:
Zs. Tóth,
zstoth@uni-bremen.de

Citation:
Tóth, Zs., V. Spiess, J. M. Mogollón, and J. B. Jensen (2014), Estimating the free gas content in Baltic Sea sediments using compressional wave velocity from marine seismic data, *J. Geophys. Res. Solid Earth*, *119*, 8577–8593, doi:10.1002/2014JB010989.

Received 27 JAN 2014
Accepted 8 OCT 2014
Accepted article online 18 OCT 2014
Published online 5 DEC 2014

Estimating the free gas content in Baltic Sea sediments using compressional wave velocity from marine seismic data

Zsuzsanna Tóth[1], Volkhard Spiess[1], José M. Mogollón[2], and Jørn Bo Jensen[3]

[1]Department of Geosciences, University of Bremen, Bremen, Germany, [2]Department of Earth Sciences - Geochemistry, Utrecht University, Utrecht, Netherlands, [3]Geological Survey of Denmark and Greenland, Copenhagen, Denmark

Abstract A 2-D high-resolution velocity field was obtained from marine seismic data to quantify free gas content in shallow muddy sediments at in situ pressure and temperature. The velocities were acquired applying Migration Velocity Analysis on prestack time-migrated data. Compressional wave velocities are highly sensitive to free gas as very small amounts of gas can cause a significant decrease in the medium velocity. The analyzed profile crosses a depression filled with organic-rich Holocene mud in the Bornholm Basin, Baltic Sea. The interval velocity field reveals two low-velocity patches, which extend from the reversed polarity reflections marking the top of the gassy sediment layer down to the base of the Holocene mud. Average interval velocities within the gassy mud are lower than the seafloor migration velocity by up to ~500 m/s. This decrease, using a geoacoustic model, is caused by an average 0.046% gas volume fraction. The interval velocities in individual cells of the velocity field are reduced to ~200 m/s predicting up to 3.4% gas content. The velocity field is limited in resolution due to velocity determination at and between reflections; however, together with the stratigraphic interpretation, geological units containing free gas could be identified. Shallow gas occurs vertically throughout most of the Holocene mud in the gassy area. Comparison with biogeochemical studies at other Baltic Sea sites suggests that the distribution of free gas is likely to be patchy in the sediment, but the gas concentration may peak below the sulfate-methane transition zone and gradually decrease below.

1. Introduction

In fine-grained sediments, methane (CH_4) is commonly produced by microbes through the degradation of organic matter. This potent greenhouse gas can be found in large amounts in unconsolidated marine sediments worldwide. Most of the methane is effectively broken down in the subsurface, either aerobically in the presence of oxygen [*Reeburgh*, 1969] or consumed by microorganisms in a process called anaerobic methane oxidation (AOM), which occurs in the sulphate-methane transition zone (SMTZ) [*Sansone and Martens*, 1978; *Reeburgh*, 2007; *Boetius et al.*, 2000; *Milucka et al.*, 2012]. Below the SMTZ, however, dissolved methane in the pore water can accumulate to levels which exceed supersaturation. Under low pressures and high temperatures typical of nonpolar continental shelves, once the partial pressure of CH_4 overcomes the ambient hydrostatic pressure, free methane gas forms as discrete bubbles.

Observations in Baltic Sea sediments suggest that free gas formation occurs in the organic-rich mud that has been deposited in the Baltic Sea since its opening to the North Sea roughly 9.8 ka [*Andrén et al.*, 2011]. Free gas has been observed in locations where this mud layer exceeds 5 to 10 m in thickness [*Thießen et al.*, 2006; *Jensen and Bennike*, 2009]. The accumulation of CH_4 gas in the sediment therefore seems to be largely controlled by sedimentation rate and the flux of organic matter to the seafloor [*Mogollón et al.*, 2012].

Little is known about the amount, vertical distribution, and migration of gas bubbles in gas-bearing marine sediments. Observational evidence provided by acoustic measurements is often restricted to imaging a snapshot in time. High-frequency sediment echosounders provide the most suitable technique for the detection and mapping of shallow gas, because acoustic signals are distinctly attenuated by the scattering of gas bubbles [e.g., *Judd and Hovland*, 1992]. Regions of shallow, gas-bearing sediments appear impenetrable in acoustic profiles, thus often blank or turbid in acoustic facies. Extensive areas of acoustic blanking and turbidity were reported and mapped in many areas of the Baltic Sea using high-frequency sources [*Mathys et al.*, 2005; *Thießen et al.*, 2006; *Laier and Jensen*, 2007; *Majewski and Klusek*, 2011]. As a consequence of the strong attenuation, however, acoustic profilers often only image the upper boundary of the gassy

sediment (gas front on top of the acoustic blanking zones) and fail to provide information about the vertical distribution of gas. Computed tomography (CT) scans of ~5 m long pressurized cores from Eckernförde Bay (Western Baltic Sea) showed that the bubble distribution in the sediment is not uniform and that gas bubbles exist within 2 to 20 cm thick intervals which are separated by gas-free intervals [*Abegg and Anderson*, 1997; *Anderson et al.*, 1998].

Transport of methane in the sediment can occur by diffusion (in the fluid phase), advection of the pore water [*Albert et al.*, 1998], or advection driven by the buoyancy of gas bubbles. Gas bubbles formed at depth may either become trapped or migrate toward the sediment-water interface [*Tréhu et al.*, 2004; *Liu and Flemings*, 2006]. Indirect evidence of bubble migration include the observation of seeps – gas bubbles rising up through the water column [e.g., *Judd*, 2004], and migration pathways observed on seismo-acoustic data, e.g., columnar disturbances and gas chimneys [e.g., *Judd and Hovland*, 1992]. Mechanisms for gas bubble formation and migration within "impermeable" mud are currently subject to debate. Gas injections into gelatine and mud showed that bubbles grow as highly eccentric oblate spheroids (disks) by fracturing the cohesive host medium or by reopening preexisting fractures [*Boudreau et al.*, 2005]. Likewise, computer simulations suggest that sediment fracturing may also trigger bubble rise [*Algar et al.*, 2011]; however, the estimated rising speeds of bubbles may be unrealistically high [*Boudreau*, 2012].

The quantity of free gas in the sediment is difficult to measure, because methane degasses when the sediment is brought to ambient pressure during core recovery. Pressurized core samplers, which could maintain the in situ gas content, are often not long enough, expensive and only rarely used [e.g., *Best et al.*, 2004]. A simple technique for measuring in situ gas concentration would thus have great advantages. In deep sea sediments, hydrate and free gas contents have been previously estimated using seismic velocities [*Lee et al.*, 1993, 1996; *Wood et al.*, 1994; *Ecker et al.*, 2000]. At low (seismic) frequencies, a small amount of free gas in the sediment reduces compressional wave velocity significantly [*Anderson and Hampton*, 1980b]. The acoustic impedance contrast between the fully water saturated and the gas-bearing sediment layers results in a reversed polarity reflector in marine seismic profiles. Based on a reduction of compressional wave velocity in gassy sediments, in situ amounts of free gas may be estimated using the velocity field obtained from seismic data.

Our goals in this study, using a 2-D shallow seismic profile from the Bornholm Basin, Baltic Sea, are (1) to investigate shallow gas-bearing sediments and the geological background of free gas formation, (2) to obtain compressional wave (seismic) velocity and estimate the free gas content in the sediment, and (3) to characterize the vertical distribution of gas bubbles in the sediment.

2. Bornholm Basin

The Bornholm Basin is located in the southern Baltic Sea, northeast of Bornholm island (Denmark), and southwest of mainland Sweden (Figure 1). This sub-basin of the Baltic Sea is situated in a major structural depression that subsided during the deposition of Upper Cretaceous sediments [*Sviridov et al.*, 1995]. The pre-Quaternary bedrock in the basin consists mainly of these late Mesozoic limestones topped with an unconformity surface, and the Quaternary basin fill is composed of a unit of glacial deposits, overlain by a succession of late- and post-glacial lacustrine and marine sediments [*Kögler and Larsen*, 1979].

After the last deglaciation of the Baltic Sea basin, isostatic uplift together with eustatic sea-level changes resulted in four to five distinct phases of sedimentation [*Björk*, 1995; *Andrén et al.*, 2011] (Figure 2). In the Baltic Ice Lake stage (BIL, 16.0–11.7 ka BP), glacial (varved) clays and silt were deposited conformably on the rugged pre-Quaternary surface shaped by glacial deformation and on top of the glacial till. The partly brackish Yoldia Sea stage (11.7–10.7 ka BP) and the fresh-water Ancylus Lake stage (10.7–9.8 ka BP) were characterized by the deposition of homogeneous clays (AY clays), which together with the BIL clays form an almost continuous cover over the deeper part of the eastern Bornholm Basin [*Kögler and Larsen*, 1979]. The beginning of the subsequent brackish Littorina Sea stage (9.8 ka BP) is a sharp litostratigraphic boundary with a change to deposition of fine-grained mud, rich in organic matter. The organic carbon content (TOC) measured in core samples shows an increase from the start of the initial Littorina Sea stage and has a maximum in the end of post-Littorina Sea (6–7%) [*Andrén et al.*, 2000]. The transition to the recent Baltic Sea stage (circa 800 B.P. to present) is recorded as a biostratigraphical change in the mud [*Andrén et al.*, 2000].

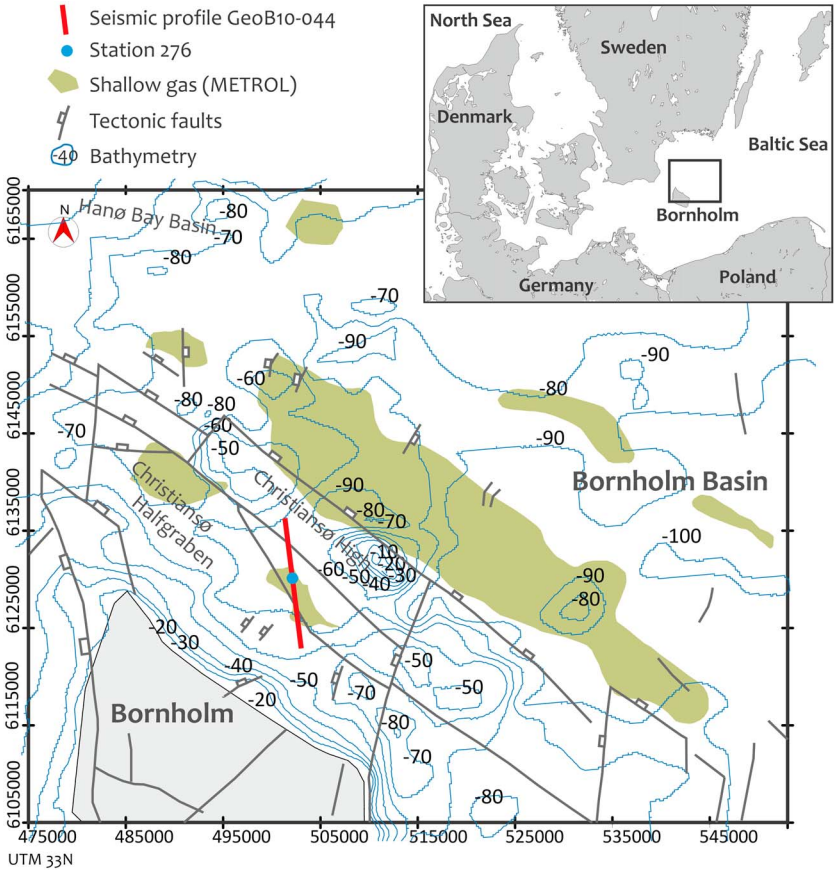

Figure 1. Location of the seismic profile GeoB10-044 in the Bornholm Basin, Baltic Sea. Green color denotes areas with free shallow gas in the Holocene mud. The seismic profile crosses the small shallow gas patch in two parts. The water depth is given in meter next to the contour lines. The map was compiled after *Vejbæk* [1985], *Laier and Jensen* [2007], and *Graversen* [2009].

Degradation of organic matter has produced CH_4 predominantly in the Littorina mud (Figure 2). Free methane gas is observed in the basin where the thickness of the mud exceeds 5–10 m [*Kögler and Larsen*, 1979]. These areas were mapped and compiled during the METROL project (http://metrol.mpi-bremen.de/) based on the observation of acoustic blanking and acoustic turbidity in high-frequency echosounder data [*Laier and Jensen*, 2007]. Shallow gas occurs in an extensive area in the eastern part of the basin and in smaller patches nearby (Figure 1).

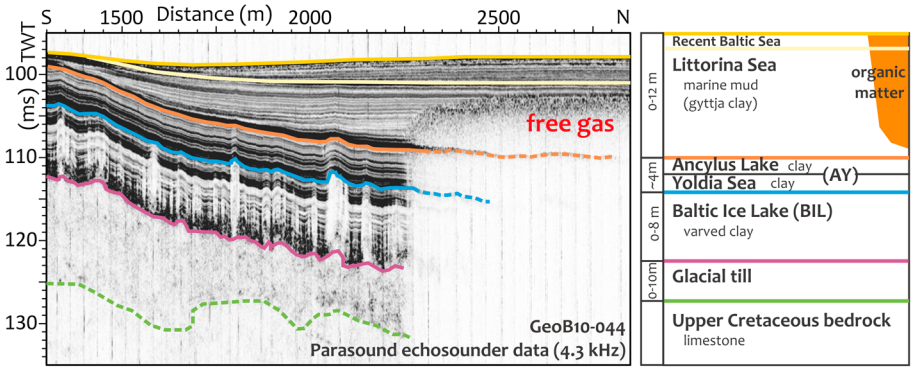

Figure 2. Stratigraphy of the Quaternary sediments in the Bornholm Basin after *Kögler and Larsen* [1979]; *Andrén et al.* [2000] represented on the 4.3 kHz Parasound data (part of the profile GeoB10-044).

3. Data and Methods

3.1. Seismo-Acoustic Data

The seismic data used in this study were acquired in August 2010 on the R/V Maria S. Merian cruise MSM 16/1, a major field campaign of the project Baltic Gas (http://balticgas.au.dk/). We selected profile GeoB10-044 from the western part of the Bornholm Basin for detailed analyses (Figure 1). The seismic data were recorded with the GeoB high resolution shallow water multichannel seismic (MCS) system, which includes a micro GI air gun (Sodera) with reduced chamber volumes of 0.1 l, and a 50 m long analog streamer with 48 channels and 1 m channel spacing comprising single hydrophones. The central frequency of the source is around 200 Hz, while the useful frequency content recorded with the streamer ranges from approx. 100 to 600 Hz. The shot rate was set to 1.5 s, average speed of the ship during the survey was ~4 knots. The MCS data were recorded with the acquisition software MaMuCS (developed by Hanno Keil, University of Bremen), with a sampling rate of 100 μs and recording length of 1.3 s. For receiving high-precision coordinates, a differential GPS (Trimble, precision ~1m) was used, whose two antennas were installed on the navigation deck of the ship.

High-resolution sediment echosounder data were acquired in parallel with the ship's parametric narrow beam echosounder Parasound DS3 (PS). Parasound emits both primary and secondary signals within a cone of only 4° opening angle, which ensures very high lateral resolution by considerably reducing the area of the reflecting surface. The transducers of Parasound are mounted to the ship's hull and simultaneously emit pulses at 19.2 kHz and 23.5 kHz, and parametric secondary frequencies are generated in the water at 4.3 kHz and 42.7 kHz. We complemented the seismic data with the 4.3 kHz echosounder data in this study. For display and interpretation of the seismo-acoustic data, we used the commercial software package KINGDOM (IHS Global Inc.).

3.2. Seismic Processing and Velocity Determination

The MCS data set was processed using the software package VISTA 2D/3D Seismic Data Processing (GEDCO). Seismic data processing partly followed a conventional marine processing flow including common midpoint (CMP) binning, spherical divergence correction, bandpass filtering, normal moveout (NMO) correction, noise attenuation and correction of residual statics (Figure 3). The geometry (source and receiver positions) was calculated from the GPS data using the custom software WinGeoApp. The CMP binsize was chosen to be 1 m to yield high horizontal resolution, which resulted in an average fold of eight.

The preliminary velocity analysis was carried out with the Interactive Velocity Analysis tool of VISTA, where the velocities of reflectors are picked at selected CMPs along the profile based on previously generated velocity semblance, common-offset stacks (COS), and constant velocity stacks (CVS), which all cover the possible range of true velocities. The root-mean-square (rms) velocities are best picked here for reflectors, where it is possible to fit the hyperbola to the travel time trajectories with certainty, aided by the velocity semblance and the CVSs. Having the aim of NMO correction, the rms velocities picked here allow the optimal stacking of traces in the CMPs, thus providing the best quality stack (stacking velocities). The resulting velocity field is, however, limited in resolution and vertical extent, because the velocity can only be picked at the first few prominent reflectors.

In order to refine this initial velocity field, we carried out a second, migration velocity analysis (MVA) (Figure 3). In principle, rms velocities are most appropriately estimated from prestack time-migrated (PSTM) data and the acquired migration velocity is, in theory, the medium velocity independent of the dip of the reflecting interface [*Yilmaz*, 2001]. As opposed to the stacking velocity estimation, where the moveout correction is done in individual CMPs, the MVA requires the complete prestack data, because the process of migration moves energy spatially from one CMP location to the other. So for the MVA, the entire prestack seismic profile was time-migrated varying the stacking velocities by 1% each time between 80 and 120%. The rms velocity functions were picked again in the Migration Image Velocity Analysis tool of VISTA, where the best "image velocity" was selected for every reflector. Figure 4 shows the velocity picks on an example CMP migrated with the different percentages of the stacking velocities. Picking is partly subjective, because it is simply a matter of deciding which velocity gives the best image at each time, but when the velocity in the migration equals the medium velocity, the event is well-compressed (the diffraction hyperbola is collapsed to its apex). Therefore, the correct migration velocity can be estimated by evaluating the quality of focusing and by choosing the best value between undermigrated (too low velocity) or overmigrated

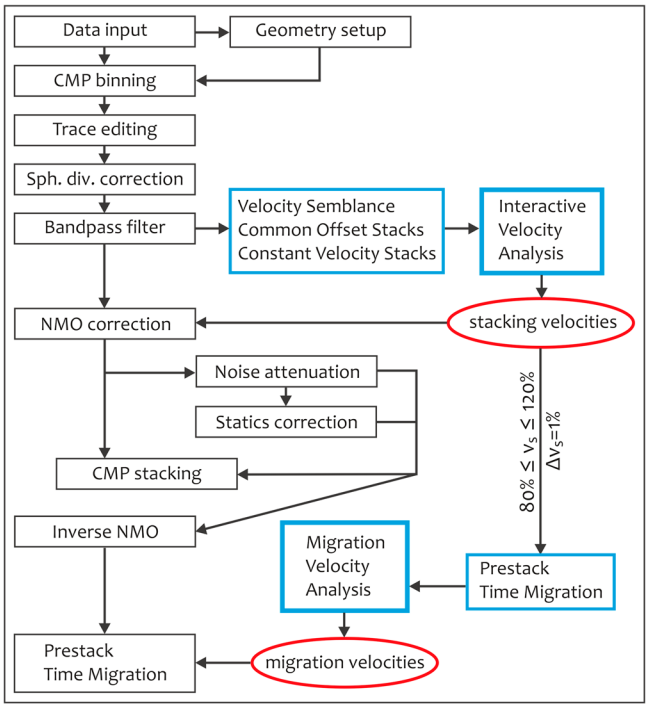

Figure 3. Flowchart of the marine seismic data processing applied to profile GeoB10-044. Apart from the conventional Interactive Velocity Analysis, a second velocity analysis was carried out using prestack time migration, which resulted in a detailed migration velocity field.

(too high velocity) events. A priori knowledge about the type of sediments and possible gas content inferred from gas signatures help as well to reach the correct velocity functions.

The seismic profile significantly improved with the migration velocities in the final prestack migration. Finally, the obtained rms migration velocities were converted into a physical interval velocity model (output of VISTA) using the Dix conversion [*Dix*, 1955].

3.3. Geoacoustic Model for Estimation of the Gas Content

The comprehensive theory of *Anderson and Hampton* [1980a, 1980b] along with analogue laboratory experiments show that the sound speed, attenuation, and reflectivity of gassy marine sediments can be dominated by the resonance of gas bubbles. Gas bubbles in marine sediments resonate at a fundamental frequency, and as a consequence, the acoustic response of gassy sediments is dependent on frequency. The relatively low frequency of the seismic source, 200 Hz, used in our survey is well below the resonance frequency of gas bubbles. Assuming typical bubble sizes of 0.5–5 mm, bubble resonance frequencies for Bornholm Basin sediments (~90 m water depth) are at $f_0 \cong 1.8$–18 kHz [based on *Anderson and Hampton*, 1980b; *Wilkens and Richardson*, 1998]. Seismic wavelengths are considerably greater than the range of bubble sizes; therefore, only the bulk properties of the medium contribute to the acoustic response of the sediment. The sediment acoustic behavior below the resonance frequency of gas bubbles is described by the Anderson & Hampton model, which relates the compressional wave velocity (v) to the bulk elastic properties (K and G) and density (ρ_s) of the sediment. It includes the modifying effect of free gas on fully saturated sediments by introducing a "compressible fluid" (for the model equations, see the Appendix). We use this model to estimate the gas content from the interval velocities obtained from the seismic data.

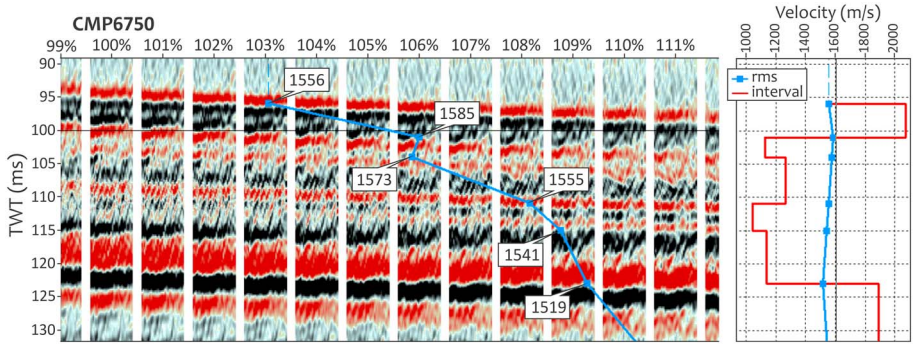

Figure 4. Migration Velocity Analysis for CMP 6750 inside the northern part of the gas patch. The 100% panel shows the prestack time migrated data using the initial stacking velocity field, while the other panels were generated using velocity fields where the initial velocity values for all reflectors were changed by the percentages given above the panels. The migration velocities, picked by selecting the best migration velocity for each reflector, is indicated by the blue curve across the panels and to the right. Interval velocities between the velocity picks are shown by the red line.

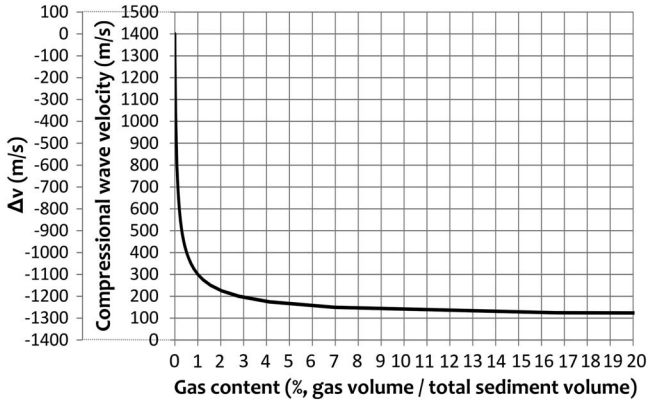

Figure 5. The relationship between compressional wave velocity and gas content in the compressible fluid model of *Anderson and Hampton* [1980b]. Same values were used for this plot as listed in Table 1. The curve shows the gas content in muddy sediments, 3 m below sediment surface in a water depth of 73 m.

In the model, the sediment is described as a comparatively stiff saturated material. Bubbles are larger than the sediment pore spaces, and they replace sediment grains (Type III, sediment displacing bubbles in *Anderson et al.* [1998]); thus, the sediment framework is deformed. The overall gas content is small and thus the expansion due to free gas is minimal. It is assumed then that greater compressibility of the gas increases the compressibility of the pore water without changing the mineral and frame compressibility and shear rigidity. Therefore, the sound speed can be derived from the stiff saturated sediment, where the bulk modulus of the pore water is modified by the bulk modulus of gas. Using this "compressible fluid model," compressional wave velocity in gassy marine sediments is predicted to decrease rapidly with increasing gas content at frequencies well below resonance. Gas content as low as 1–2% reduces the velocity by several hundreds of m/s (Figure 5).

The physical property values used in the calculation of the gas content are listed in Table 1. The sediment bulk density and porosity are average values from measurements on samples of gravity cores along the profile, which were taken on an earlier cruise (R/V Gunnar Thorson cruise in 2004, project METROL) [*Fossing*, 2005a]. The mineral bulk modulus and sediment shear modulus values were taken from the study of *Wilkens and Richardson* [1998]: the latter was measured in the Eckernförde Bay, Baltic Sea. The value of the sediment frame bulk modulus is from the table of *Anderson and Hampton* [1980b] regarding sound speed and frame elastic properties (Part II, Table III).

4. Results

4.1. Interpretation of the Seismo-Acoustic Data

The 13 km long profile GeoB10-044 crosses twice a small mud-filled depression with free gas in the western part of the Bornholm Basin (Figure 1) and reveals along the profile two, 2–3 km long gas patches (Figure 6), which are actually the southern and northern lobe of the same small gas patch. In the high frequency PS data (Figure 6a), the gassy sediment is clearly recognizable as zones of acoustic blanking. The acoustic blanking is caused by the strong attenuation of the high-frequency acoustic signal due to absorption and scattering of gas bubbles in the sediment. As a consequence, only the top of the free gas layer, the gas front, is imaged and reflections are almost completely absent beneath. The reflection from the surface of the AY clays, probably due to the large acoustic impedance contrast, remains traceable near the edges of the blanking zones, but no reflections are visible further toward the center. The gas front in the PS data appears in the mud at depths ranging from ~7.0 to 2.0 and 4.5 to 3.8 m in the southern and northern patches respectively.

Table 1. Values of Parameters Used to Calculate Gas Content, Methane Solubility, and Methane in Gas in the Gassy Sediments of the Bornholm Basin

Shear modulus of the sediment (G)	2.81×10^5 Pa [a]
Sediment bulk density (ρ_s)	1.35×10^3 kg/m^3 [b]
Mineral particle bulk modulus (K_m)	3.6×10^{10} Pa [a]
Sediment frame bulk modulus (K_f)	1.4×10^7 Pa [c]
Fractional porosity (n)	0.8 [b]
Pore water bulk modulus (K_w)	2.14×10^9 Pa
Ratio of specific heats of gas (γ)	1.31
Hydrostatic pressure at 1 atm (P)	1.01325×10^5 Pa
Seawater density (ρ_w)	1.013×10^3 kg/m^3
Temperature (T)	$6.5°C$

[a] *Wilkens and Richardson* [1998].
[b] *Fossing* [2005a].
[c] *Anderson and Hampton* [1980b].

This gas front is not clearly visible on the multichannel seismic data (Figures 6b and 6c). Only on close inspection, it can be seen that the gas front is a separate, negative polarity reflector having a peak-trough wavelet shape as opposed to the

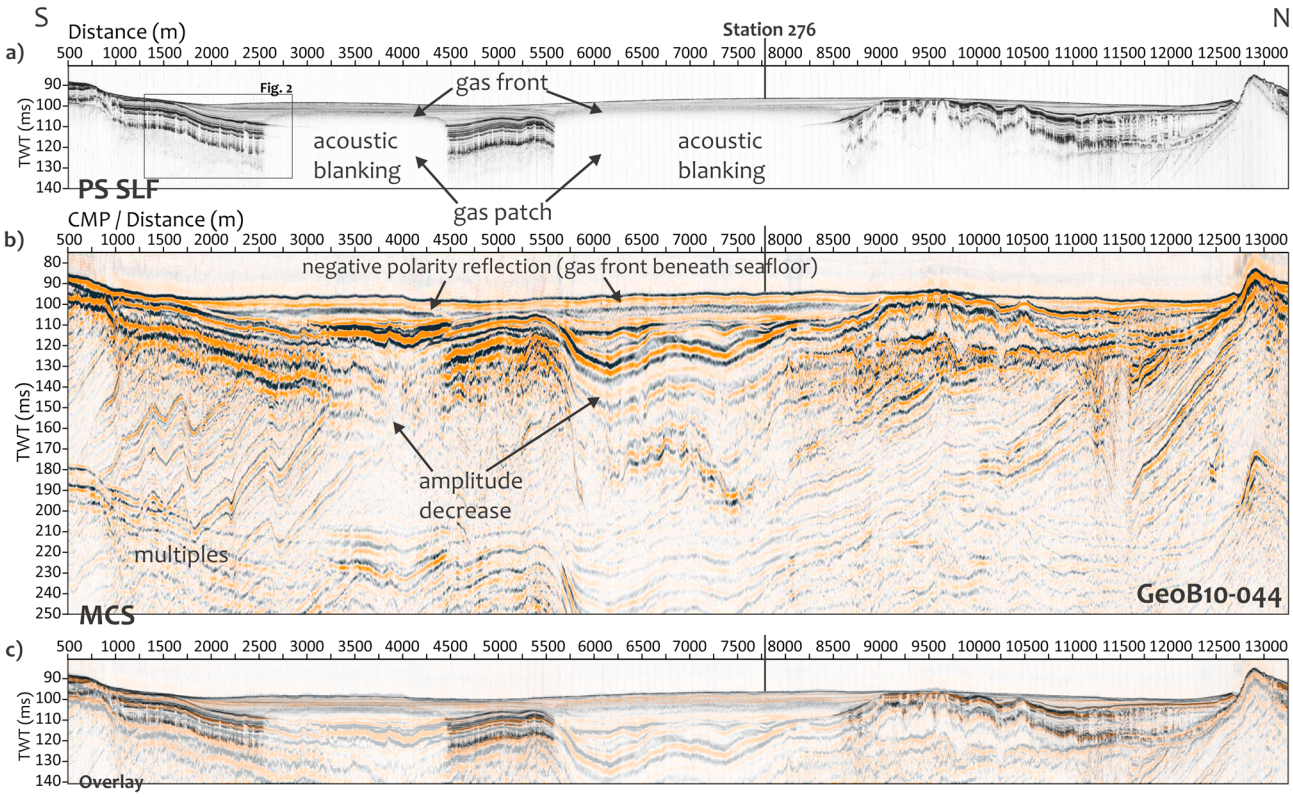

Figure 6. Profile GeoB10-044, (a) Parasound SLF data (4.3 kHz, envelope display), (b) multichannel seismic data, and (c) their overlay. The seismic profile crosses one small gas patch in the Bornholm Basin twice. The vertical exaggeration is ~58×. For the location of the profile, see the map in Figure 1; the stratigraphical interpretation of the data is in Figure 7.

positive trough-peak wavelet of the seafloor reflection. The reversed polarity is the result of a decrease in acoustic impedance (reduced compressional velocity and lower density) due to the presence of free gas. Toward the edges of the gas patches, where the sub-bottom depth of the gas front gradually increases, the separation is somewhat clearer. Elsewhere, the reflections of the seafloor and the gas front merge.

Beneath the negative polarity gas reflections, two depressions are revealed by the MCS data (Figures 6b and 7). The shape of the southern depression is easier to infer from the base of the AY-BIL clay layers which conformably cover the eroded surface of the bedrock. However, beneath the northern part of the gas patch, a deep glacial valley is exposed (Figure 7). While the AY clays form only a thin layer in both depressions, the seismic unit identified as BIL clays appears thicker toward the north.

Beneath the reversed polarity reflector representing the gassy layer, the seismic data show one or two more, roughly horizontal reflectors in the otherwise acoustically transparent mud layer (Figure 6b). They have a low-amplitude, rather disturbed and fuzzy seismic appearance, and it is hard to determine whether they have normal or reversed polarity due to possible interference, although the first positive peak seems more pronounced suggesting a decrease in acoustic impedance. In the southern part of the depression, this is coupled with a very high amplitude reflection at the base of the Holocene mud. Here, the significant amplitude increase can be the result of constructive interference between a reflection in the mud and the underlying reflector of the AY clays.

4.2. Interval Velocities

The interval velocity field obtained from the MCS data is displayed in Figure 8a with the velocity picks at the selected CMP locations. For a sediment layer or unit, the interval velocity is calculated between the reflectors at which the rms velocities were picked, and determination of a layer interval velocity requires a reflector/pick at the base. Interval velocities are displayed without any interpolation or smoothing. Therefore on Figure 8a, cells defined by the velocity picks are colored based on the interval velocity values within them.

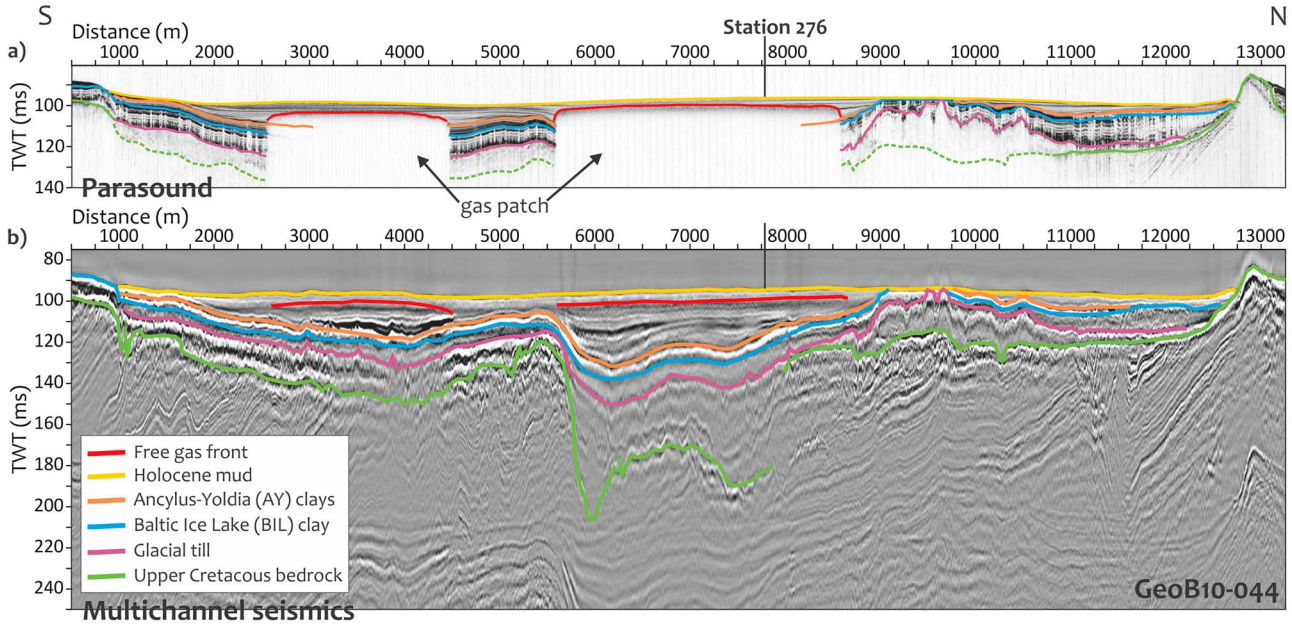

Figure 7. Interpretation of profile GeoB10-044, (a) Parasound SLF (4.3 kHz, envelope display), and (b) multichannel seismic data. The vertical exaggeration is ~58×. Location of the profile is in Figure 1.

The horizontal boundaries of these cells are the picks/reflectors (indicated in the middle of the cell), and the vertical boundaries are the CMPs where the velocities were picked. The two low velocity patches between CMPs 2500–4500 and 5500–8500 in the vertical range of 105–130 ms TWT are evident. The top of these low velocity zones coincides with reversed polarity reflections verifying the decrease in acoustic impedance as

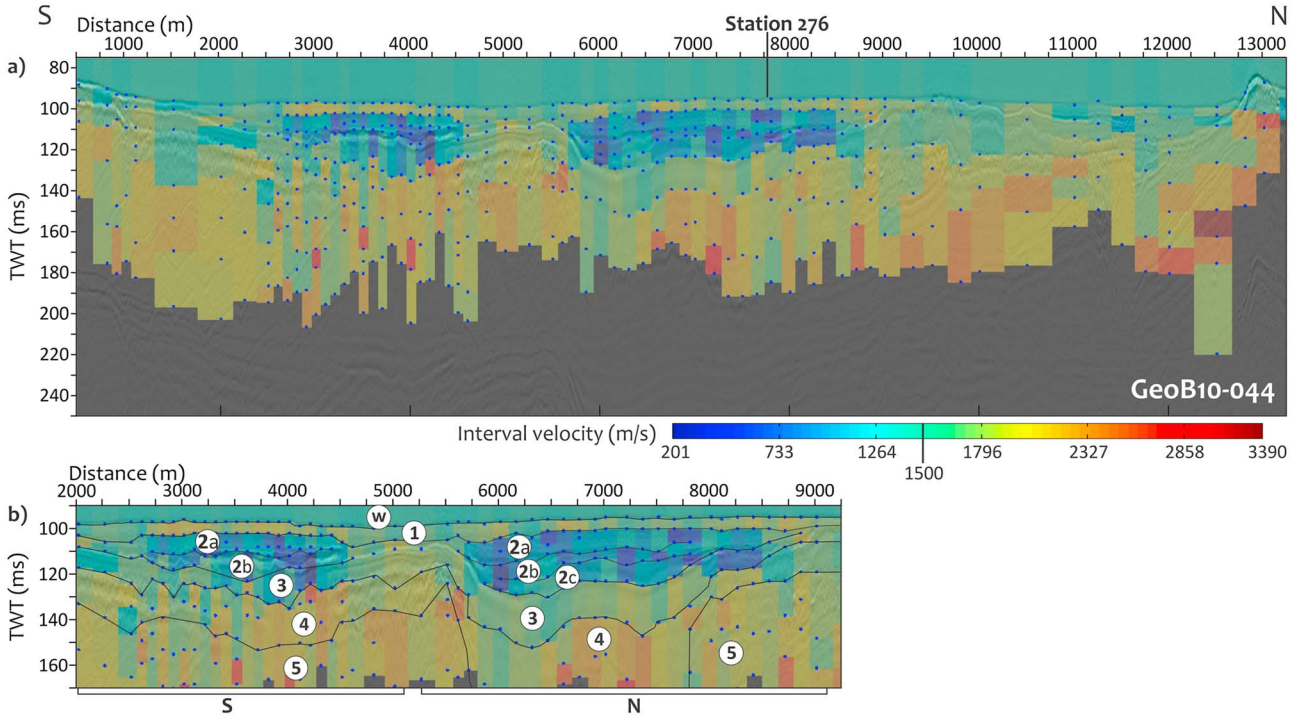

Figure 8. (a) Interval velocities superimposed on the seismic traces of the profile GeoB10-044. The velocity picks from the Migration Velocity Analysis are indicated with blue dots in each CMP where the velocity of reflectors were picked. The picks and CMPs define cells, which are colored respective to the interval velocity values in them. (b) A close-up of the two parts of the gas patch with the layer boundaries, where average interval velocities were calculated.

Table 2. Average Interval Velocities in the Layers in Figure 8b, the Average Two-Way Travel Time of the Bottom of the Layers, Their Depth, and Gas Content Calculated Based on the Compressible Fluid Model[a]

Layer		TWT (ms)		Depth (m[b])		Interval Velocity (m/s)		Δv (m/s)		Gas Content (%)	
water column		96		73.92		1540		0		0	
layer 1	(gas-free mud)	102		78.54		1902		361		0	
		S	N	S	N	S	N	S	N	S	N
layer 2a	(gassy mud)	110	110	84.7	84.7	1184	1223	−356	−317	0.04	0.03
layer 2b	(gassy mud)	119	119	91.63	91.63	1164	1040	−376	−500	0.04	0.07
layer 2c	(gassy mud)		122		93.94		1129		−411		0.05
layer 3	(clays)	130	132	101.1	101.64	1700	1678	159	138	0	0
layer 4	(till, valley fill)	144	144	110.88	110.88	2055	2177	515	637	0	0
layer 5	(bedrock)	185	175	142.45	134.75	2198	2162	657	622	0	0

[a]S the layers within and below the southern part of the gas patch, N the ones in the northern part of the gas patch.
[b]v = 1540 m/s.

indicated by the polarity change (Figure 6). The interval velocity inside the patches varies between a minimum of 200 m/s and a maximum of 1400 m/s. These low velocities confirm the presence of free gas in the sediment.

The interval velocity is highly variable laterally within layers and stratigraphic units. To gain a better representation of the interval velocities in each stratigraphic unit and the distribution of free gas, average values were calculated around the two parts of the gas patch for layers 1, 2a–2c, 3, 4, and 5 as shown in Figure 8b (Table 2). Based on the reflections where the velocities were picked in the Holocene mud unit, layer 2 (gassy mud) was divided into two and three sublayers in the northern and southern part. These reflections in the mud occur probably due to changes in grain size. The interval velocities averaged horizontally within the layers, split between the northern and southern part of the gas patch, are summarized in Figure 9.

The first picks at the seafloor determine the sound speed in the water column (w), which is around 1540 m/s. The average interval velocity in layer 1, which encompasses the sediment from the top of the mud layer to the gas front (thus gas-free), is 1902 m/s. This is anomalously high as expected velocities for a high-porosity surficial muddy sediment are close to sound speed in seawater or even lower due to the low rigidity and high compressibility of water, so $\leq$1450 to 1500 m/s. The low-velocity zones in the mud (layers 2a–2c) have average interval velocities here ranging from 1040 to 1223 m/s, consistent with velocity decrease caused by free gas. Beneath these zones, the interval velocity of layer 3 is 1700 m/s, which corresponds to the dense clays beneath the mud. Layer 4 below (glacial till) and layer 5 (bedrock) reach interval velocities of 2055–2198 m/s.

4.3. Gas Content

Finally, using the compressible fluid model, we calculated the free gas content (n_g, gas porosity = gas volume/total sediment volume) based on the average interval velocities of the layers. Since the relative gas content is dependent on the ambient hydrostatic pressure, for each layer an average depth was used in the calculation (Table 2). The relationship between compressional wave velocity and gas content is shown in Figure 5. This curve was plotted for typical muddy sediments of the Bornholm Basin, 3 m below the sediment surface in a water depth of 73 m. Even very small amounts of gas cause a significant decrease in the compressional wave velocity: 0.1% gas volume is associated with a 50% drop, 1% decreases the velocity to 300 m/s and 3% to only 200 m/s (Figure 5).

Based on the compressible fluid model, compressional wave velocity would be 1400 m/s in a muddy seabed sediment with zero gas content and physical properties listed in Table 1 (Figure 5). Since this is lower than the velocity measured for seabed sediments, we modify the calculation of the gas content using the velocity drop (Δv) with reference to a gas-free seabed sediment velocity of 1540 m/s. Any decrease of the average migration rms velocity is then attributed to the presence of gas (Table 2). Accordingly, the velocity drop in layers 2a–2c is caused by 0.03–0.07% gas in the sediment (by volume) within the respective layers. The average gas content in the Holocene mud, according to the compressible fluid model, is therefore 0.046% overall.

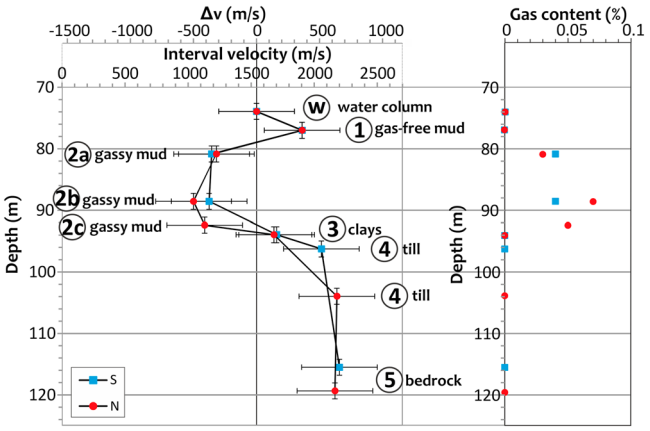

Figure 9. On the left-hand side, the average interval velocities of the layers denoted in Figure 8b is plotted separately for the northern and southern part of the gas patch. The water velocity is indicated with the vertical line at 1540 m/s. The interval velocities of layers 2a–2c on the left of this line indicate the presence of free gas. These layers correspond to the Holocene mud below the gas front. The bars indicate the error ranges of the interval velocity. On the right: gas volume fractions in layers 2a–2c derived from the velocity change based on the Anderson and Hampton model.

5. Discussion

5.1. Uncertainty of the Interval Velocities

The accuracy and resolution of velocity estimations from seismic data depends on several factors. Since velocity is determined directly from the data, both the setting and the equipment determine accuracy and resolution. The source frequency and data bandwidth define the basic resolution. The water depth together with the offset (streamer length) and the ship's speed influence the fold and the measurability of hyperbolic move-out. The signal-to-noise ratio in the data influences the overall accuracy.

The main error sources in the velocity determination are the parameters that influence the travel time. These parameters are related to the positional geometry of the source and the receivers. While a centimeter accuracy is realizable in measuring the momentary distances of the source and receiver positions (both horizontally and vertically), these are measured once and assumed to be constant during the entire survey. Nevertheless, variable weather and oceanographic conditions, as well as waves and their effects on the equipment movement, may lead to relatively small scale displacements. Their effect on the velocity is difficult to estimate, because the deviation from the assumed positions is unknown. Additionally, the "gun delay," the time between the trigger signal and the actual release of the air bubble into the water, is usually either roughly estimated from the data or imposed empirically. Ultimately, the geometry, gun delay, and thus the velocities can be calibrated with the velocity of the direct wave, which must be close or equal to the speed of sound in water.

Furthermore, errors in the determination of interval velocities may result from uncertainties in the rms velocity measurements. The travel time errors are secondary in the derivation of interval velocities, although the effect of the timing error becomes more important at reflection times less than 1 s [*Hajnal and Sereda*, 1981]. We can estimate the error in the velocity estimates by evaluating the accuracy of the MVA method. Errors in the MVA result from the inaccuracy of velocity picking. Since the stacking velocities beforehand are varied by 1%, the error in the migration rms velocity is at least ±15 m/s. However, picking is partly subjective and the best "image velocity" can be picked from a larger range, which we estimate to be about ±2%. Therefore, the confidence range of the migration rms velocity can be estimated to be about ±30 m/s. Picking in time in the MVA has an error of about ±1 ms. These together can cause errors of as high as 300 m/s in the interval velocities (based on the uncertainty formula of *Hajnal and Sereda* [1981]). The confidence range of the best "image velocity" in the MVA gets wider at deeper reflections. This is expected as the lack of significant move-out at deeper reflections inhibits velocity discrimination. The uncertainty in the computed interval velocity of a layer will consequently increase with reflection time.

It should be also noted that the resolution of the velocity field is affected by the reflector locations where the velocity of an event can be picked. It is thus greatly influenced by the variability of the geological structure and the vertical resolution. The uncertainty in the interval velocity of a layer is inversely proportional to the interval travel time of that layer [*Hajnal and Sereda*, 1981], which in case of our high resolution picking (layer thickness of 3–4 ms TWT) may lead to larger error ranges. In summary, the interval velocity determined by MVA can have an error of 300 m/s, and its uncertainty will increase with reflection time and with decreasing layer thickness.

5.2. Variability in the Interval Velocities

Based on our MVA, the migration rms velocity of the seafloor reflection (and thus the interval velocity/sound speed in the water column) is 50–100 m/s higher than sound velocity measured near the seabed from CTD casts (1459 m/s) [*Schneider von Deimling et al.*, 2013]. Although the reasons are unclear, our higher migration velocities at the seafloor may indicate that the values of the entire velocity field are higher than the real medium velocity values.

The anomalously high average interval velocity of layer 1, corresponding to gas-free mud at the seabed, likely shows the effect of thin layers on the interval velocity. Compressional wave velocity in gas-free muddy seabed of the Eckernförde Bay, Baltic Sea (similar environment and sediment) was measured in situ using an acoustic lance and it was found to be 1430–1480 m/s [*Fu et al.*, 1996; *Wilkens and Richardson*, 1998]. The ~400 m/s deviation here is probably attributable to rms velocity picks at too close time intervals, which can yield anomalous interval velocities from the Dix conversion, even though the increase in rms velocity with depth is small [*Yilmaz*, 2001]. For example, in the case of rms velocities of 1500 and 1550 m/s at the top and base of a 3 m thick layer (4 ms TWT), the interval velocity is 2452 m/s. Therefore, the 1902 m/s interval velocity of layer 1 is a consequence of the vertically high resolution velocity picking and the derivation of the interval velocity, and it does not characterize the sediment layer between the bounding rms velocity picks. Similarly, the interval velocity can be anomalously low when the bounding rms velocity picks are too close to each other and the rms velocity decreases too sharply between the two picks. To avoid the thin layer problem or the too sharp decrease of the rms velocity, we ran tests to investigate the reliability of the interval velocity values by removing velocity picks within the gassy sediment. These showed that the lowest velocities inside the gassy mud are not anomalous. Nevertheless, it is important to note that as the layer thickness decreases, the uncertainty in its interval velocity will increase.

The interval velocities within layers/stratigraphic units (Figure 8a) appear highly variable. This variability can result from the method of velocity determination and/or could reflect small changes in the sediment lithology, gas content, etc. While such significant changes in lithology within stratigraphic units are not likely in Bornholm Basin sediments, variations in layer thickness and depth can result in slightly different interval velocities. In the Dix conversion, the underlying assumption is that the earth model comprises horizontal isovelocity layers. Therefore, decreasing layer thicknesses lead to increasing interval velocities and larger uncertainties in the computed interval velocities of the deeper layers. As a consequence, the interval velocity determined between closely spaced reflectors in a complex geological structure will likely result in highly variable values.

Apart from this, variability in the distribution, amount, and concentration of gas bubbles may also cause subtle changes in the compressional wave velocity. *Abegg and Anderson* [1997] found in the Eckernförde Bay sediments that gas bubble distributions are variable vertically on a centimeter scale (thin gassy and nongassy layers a few cm thick in 5 m long cores) and horizontally on a meter scale (from cores collected 2–20 m apart). Actual gas volume concentrations measured in cores kept under in situ pressure and temperature using the CT scanning technique revealed highly variable free gas concentrations, from 0.1% to 9%, changing both vertically and laterally [*Abegg and Anderson*, 1997; *Anderson et al.*, 1998]. This means that alternating layers of low and high velocities in the sediment are likely [*Wilkens and Richardson*, 1998]. While high concentrations of gas bubbles represent small heterogeneities in the medium when compared to the wavelength of the seismic wave (the wavelength $\lambda \sim 7.5$ m for the 200 Hz signal of the airgun), given the high sensitivity of compressional wave velocities to changing gas content (Figure 5), thin gassy sediment layers can cause considerable variability in the interval velocities. Measured velocities thus represent an average of lower velocities in gassy sediments and higher velocities in gas-free sediments.

5.3. Velocity Reduction–Gas Content

Gardner [2000] performed controlled experiments on silty clay samples prepared in the laboratory containing 1–2% gas volume with a uniform distribution of 0.2–1.8 mm sized gas bubbles. The acoustic response of the gassy sediments was broadly as predicted by the compressible fluid model, with measurements of compressional wave velocities as low as 220 m/s below the resonance frequency of the bubbles. However, a subsequent study by *Gardner and Sills* [2001] revealed that velocities based on bulk properties of sediments containing "large bubbles" match the actual velocity measurements better than velocities based on the predictions of the compressible fluid model. In the "large bubble model," gas is contained in structural pockets in the saturated sediment [*Wheeler*, 1988; *Wheeler and Gardner*, 1989]. This is probably a more appropriate

physical description of gas-bearing sediments, as typical gas bubbles are bigger than clay or silt particles and cannot be wholly contained within the pore water in typical fine-grained sediments. The large bubbles have a lower compressibility than the small bubbles formed within the fluid. Consequently, the velocity reduction due to free gas happens to a lesser degree, because the abrupt increase in the bulk compressibility is smaller (equation (A1) in the Appendix). This means that the reduction in the interval velocities might be caused by an even larger amount of gas in the sediment than the compressible fluid model suggests (for more detail, see *Gardner and Sills* [2001]). Our calculated free gas contents may thus represent a lower estimate of gas contents.

Dvorkin and Nur [1998] considered different saturation patterns in partially saturated sediments and rocks. In their model, patchy gas saturation as opposed to the homogeneous pattern, is a pore fluid arrangement where the fluid (free gas) is arranged in fully saturated patches that are surrounded by dry (nongassy) or partially saturated regions. The gas saturation can be therefore heterogeneous on scales greater than the pore or grain size but on scales smaller than the seismic wavelength. If the gas saturation is patchy in the Holocene mud, then again much higher gas concentrations would be predicted from the low-velocity zones, because the increase in the bulk compressibility of the sediment is smaller than in case of a heterogeneous fluid saturation.

5.4. Gas Distribution and Amount in Bornholm Basin Sediments

The depth distribution of gas bubbles in the sediment is difficult to evaluate, because information about the free gas zone derived from seismo-acoustic data is limited. In the PS profiles, the top of the free gas zone is marked by the strongly scattering gas front, but due to the strong attenuation of the high-frequency signal, nothing deeper can be inferred from inside the acoustic blanking zones (Figure 6a). In the lower frequency seismic data, a horizon at the same depth as the gas front in PS data appears as a reversed polarity reflection (Figure 6b), and although penetration through the gassy layer is achieved, the base of the gas-charged sediment layer is difficult to identify. If the gas bubbles are concentrated in a thin layer, it might not be possible to resolve the layer boundaries as separate reflections. If the gas bubbles are distributed in a thicker layer, but with a gradual decrease of gas bubble concentration with depth, then again only one reflection may be observed, which would then mark the top of the gas-charged sediment layer. The gradual increase of velocity and/or density (gradient zone) in the medium will not cause a sharp acoustic impedance contrast; thus, reflection amplitude may be much lower than expected from the total impedance contrast.

The interval velocity field determined from the MCS data (Figure 8a) reveals presence of free gas through the reduction of compressional wave velocity ($v < 1540$ m/s, blue colors). Low interval velocities characterize the Holocene mud layer beneath the gas front. The velocity drop is confined to the mud (layers 2a–2c), whereas the clays below (layer 3) show higher interval velocities well above 1540 m/s (Figure 8b and Table 2). This suggests that gas bubbles are present throughout the Holocene mud beneath the gas front. The velocities for all layers represent average values for these units and thus do not take into account any intralayer vertical variations and inhomogeneities. Also, the long seismic wavelength and the vertical uncertainty of the reflector picks limit the velocity resolution for thin layers. Accordingly, the velocity drop with respect to the velocity in gas-free sediment (the reference value) probably indicates average free gas content. The average interval velocities in layers 2a–2c suggest that in the northern part of the gas patch the highest free gas concentrations occur in the middle of the mud unit. This is not well resolved in the southern part of the gas patch, where the two layers in the mud unit appear to have similar gas contents.

Multicore data retrieved from the northern part of the gas patch [Station 276, latitude: 55.317950°N, longitude: 15.028730°E, water depth: 73.2 m, *Fossing*, 2005b] reveal that the SMTZ is located at a depth of approx. 30 cm below seafloor (Figure 10). This SMTZ depth is not uncommon for gassy sediments in the Baltic Sea and is similar to SMTZ depths compiled at Eckernförde Bay [*Mogollón et al.*, 2011, and references therein], and Arkona Basin [*Mogollón et al.*, 2012]. The reversed polarity reflector at Station 276 for the free gas depth occurs at 2.68 m below seafloor. The in situ pressure, temperature, and salinity conditions at this sediment depth lead to a methane solubility concentration of 16.4 mM [*Mogollón et al.*, 2013]. Combining this information, a methane gradient between the deepest methane measurement and the free gas depth is estimated to be 6.9 mM m^{-1} (Figure 10). This gradient is considerably less than that obtained from linearly interpolating the two deepest methane concentration (10.5 mM m^{-1}). This discrepancy is due to the dynamics of methanogenic and methanotrophic processes, with the steepest portion of the methane curve taking place at the change from net methanogenesis to net methanotrophy [*Mogollón et al.*, 2009].

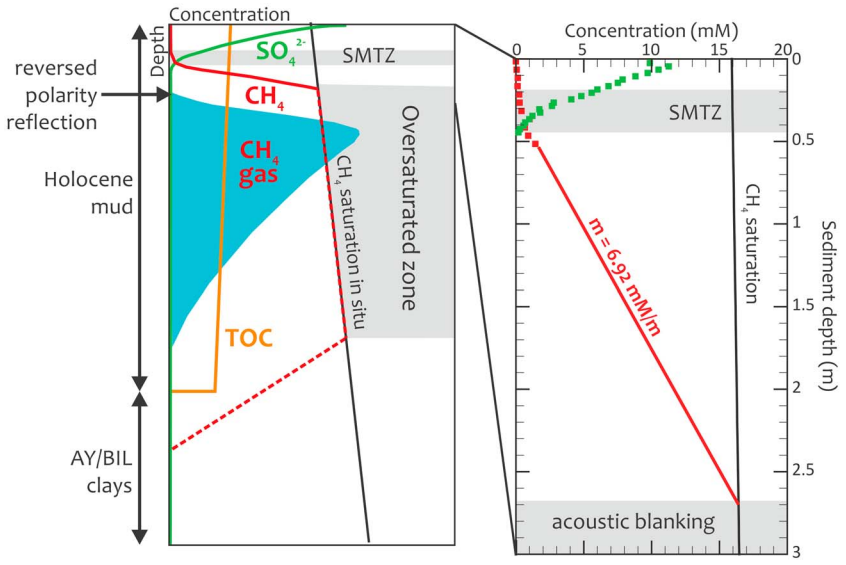

Figure 10. (left) A schematic depiction of methane cycling within the Holocene mud, showing idealized sulfate (SO_4^{2-}), methane (CH_4), and total organic carbon (TOC) concentration curves, as well as the sulfate-methane transition zone (SMTZ). The existence of CH_4 gas beneath a reversed polarity reflection is depicted by the blue region. A zone of oversaturation with respect to CH_4 is shaded grey. (right) A close-up showing measured CH_4 and SO_4^{2-} concentrations (colored dots) from Station 276 (see Figure 1 for location), put into context with the schematic panel to the left. A methane concentration gradient with respect to depth is predicted by linking the deepest measurement point to the intersection of the top of acoustic blanking with the CH_4 saturation curve (red line).

Previous studies in gassy sediments show that this switch occurs at approx. 1-3 mM methane concentrations [e.g., *Martens et al.*, 1998; *Mogollón et al.*, 2009, 2012]. In Eckernförde Bay, for example, measured profiles from *Martens et al.* [1998] show that the methane gradient decreases from 22.3 mM m^{-1} at the switch from methanotrophy to methanogenesis down to 9 mM m^{-1} at depths near the free gas depth. Nevertheless, the measured methane gradient at Station 276 falls within range of a linear best fit to the three deepest measured methane concentrations (7.75 mM m^{-1}).

The distribution of gas bubbles in the sediment is locally controlled by the methane concentration, the hydrostatic pressure, and the methane solubility (which is determined by the temperature, the hydrostatic pressure and the salinity). The methane concentration within the gas zone is controlled by the rate of (net) methanogenesis, the rate of gas production/dissolution, and the flux both up and down core. When the methane concentration exceeds the solubility concentration, a reversed polarity reflection will appear as a consequence of the bulk property change of the medium due to bubble formation.

Within the gassy zone, the free gas concentration will likely increase gradually toward a peak value with increasing sediment depth. As methane content is minimal in glacial clays, both free gas concentration, and further downward, concentration of dissolved methane, will decrease from this point following a diffusive gradient (Figure 10). The zone where gas bubbles exist can extend almost down to the base of the Holocene as these depths remain methanogenic due to ongoing organic carbon degradation. Since a minimum thickness of the methanogenic mud is required for free gas to form, the lower most section may not contain free gas [*Mogollón et al.*, 2012].

The vertical distribution of free gas probably depends on the sediment physical properties and on the local geochemistry. High variability of the interval velocities and measured gas volume concentrations might point to a patchy distribution. Nevertheless, even if not evenly distributed, free gas occurs throughout most of the Holocene mud beneath the gas front, and not only concentrated in a 1 or 2 m thick layer. If this situation is true, then there is no accumulation of free gas occurring, which would concentrate gas bubbles. The present vertical distribution is rather a snapshot of a system in equilibrium, where methane production, migration, gas formation, and methane consumption are ongoing and shape both the dissolved methane and free gas concentration curves.

The average gas content of 0.046% for the Holocene mud from our calculation is comparable with the results of other studies from the Baltic Sea. Methane gas concentrations at in situ pressure and temperature have been measured in the muddy sediments of Eckernförde Bay. Over the depth zone of 50 to 120 cm, at a water depth of 26 m, the average gas concentration was found to be approx. 0.02% [*Abegg and Anderson*, 1997; *Anderson et al.*, 1998; *Martens et al.*, 1998]. Modeling studies by *Martens et al.* [1998] and *Albert et al.* [1998], which quantitatively couple the biogeochemical processes to the input flux of reactive organic carbon in the sediment, predicted gas concentrations of ~0.3%, for essentially the same depth zone where the gas bubbles were observed in the pressurized cores. *Mogollón et al.* [2011] used a reactive transport model to investigate the seasonal dynamics of the methane cycle. Their model predicted (depth-averaged) gas volume fractions of 0.25% for the early fall months in the Eckernförde Bay sediments, and early spring values were as low as 0.021%. This model study also indicated that there can be considerable variations in the position and thickness of the free gas layer due to the seasonal fluctuations of heat propagation. This needs to be taken into account when comparing measured values of free gas concentration.

In our study, the interval velocities in individual cells of the velocity field are reduced to 201 and 262 m/s in the southern and northern part of the gas patch, respectively. This predicts up to 3.4% and 1.6% gas content in the volumes of the sediment bounded by the rms velocity picks. These values seem high compared to the average gas content, but not unlikely, as pressurized cores from the pockmark site in the Eckernförde Bay reached concentrations as high as 9%. Based on model predictions, *Mogollón et al.* [2011] argues that high free gas concentrations are unlikely near the gas front due to seasonal production and migration of free methane gas. Deeper gas layers may thus be a product of gas burial and concentration over a long period of time [*Mogollón et al.*, 2012].

Given our estimated average gas concentration based on seismic velocities, it is possible to predict gas volumes on a more regional scale if we assume that our gas content estimate is representative of the entire gas patch area. Imposing the average gas contents, depths and thicknesses for the gassy zone (layers 2a–2c, Table 2), as well as the sediment properties listed in Table 1, a depth-integrated quantity of 2.8 mol m^{-2} can be estimated for the methane gas present. Nevertheless, this value probably represents a low estimate since the model does not capture small-sized bubbles (also see discussion in section 5.3). If this value is representative for the entire gas patch area of 15.25 km^2, then around 43 Mmol methane would be harbored in the Holocene mud as free gas, or roughly 1.1×10^6 m^3 of methane at standard ambient temperature and pressure. While this constitutes a small fraction in comparison to the global methane hydrate inventory [$10^{17} - 10^{18}$ mol C, *Dickens*, 2011], it is evaluated over a gassy patch that represents only 0.00005% of the global shelf (0-200 m water depth) extent. Given the prolific evidence for free methane gas in these shallow sediments [*Fleischer et al.*, 2011], we may expect that the yet unreported free gas inventory can be a significant part of the global methane reservoir.

6. Conclusions

We performed detailed velocity analyses on a 2-D shallow marine seismic profile from the Bornholm Basin, Baltic Sea. Although it is time consuming and computationally intensive, migration velocity analysis offers a method to obtain high-resolution velocity fields from prestack time migrated data. Beyond ensuring accurate geometry and travel times in the seismic data, precise velocity determination is important, as small errors in the migration rms velocities can result in large errors in the interval velocities.

The seismic profile GeoB10-044 crosses a small depression filled with organic-rich Holocene mud, where shallow free gas is observed. Free gas in the sediment is indicated by acoustic blanking zones on the high-frequency acoustic data, and the same horizon as the gas front appears as a reversed polarity reflection on the lower frequency seismic data. The interval velocities obtained from the seismic data reveal two low-velocity zones along the profile, which extend from the reversed polarity reflections down to the base of the Holocene mud layer. Average interval velocity values within the gassy mud are lower than the seafloor migration velocity by up to 500 m/s. This decrease in interval velocity, using the geoacoustic model of *Anderson and Hampton* [1980b] that relates compressional wave velocity to sediment physical properties and gas content, is caused by an average 0.046% gas fraction in the sediment. Compressional wave velocities in the sediment are highly sensitive to free gas, and very small amounts of gas cause a significant decrease in the medium velocity at seismic frequencies. Based on the seismo-acoustic data and the

derived interval velocities, shallow gas occurs vertically throughout most of the Holocene mud. Although the distribution of free gas is patchy in the sediment, the gas concentration is likely to have a peak below the sulphate-methane transition zone and gradually decreases below.

Interval velocities obtained from multichannel seismic data can be used for the assessment of free gas concentration at in situ pressure and temperature in shallow marine sediments. The measurement of the velocity reduction caused by free gas is possible even when only a small amount (>0.01%) of free gas is present in the sediment. The high-resolution velocity field offers the opportunity to investigate the free gas distribution with depth as well. Although limited in resolution because of the requirement of reflectors, together with the stratigraphic interpretation of the seismic data, geological units containing free gas can be identified. Due to the frequency dependence of gas-bearing sediments and the seismic method, relatively low source frequency is needed, which is well below the resonance frequency of gas bubbles and provides penetration through the gassy sediment layer, but sufficiently high as to provide high vertical resolution in the imaging of the subsurface.

Appendix A: Geoacoustic Model

The relationship between compressional wave velocity and the physical and elastic properties of gas-bearing sediments at acoustic frequencies much less than the bubble resonance frequency is given by the following equations after *Anderson and Hampton* [1980b] and *Wilkens and Richardson* [1998].

Compressional wave velocity in gas-bearing sediments is given by the wave equation:

$$v = \sqrt{\frac{K + \frac{4}{3}G}{\rho_s}}, \tag{A1}$$

where K is the bulk modulus of the gas-bearing sediment, G is the sediment shear modulus, and ρ_s is the sediment bulk density. The sediment composite bulk modulus is calculated based on Gassmann's expressions [*Gassmann*, 1951]:

$$K = K_m \left(\frac{K_f + Q'}{K_m + Q'} \right), \tag{A2}$$

where

$$Q' = K'_w \left(\frac{K_m - K_f}{n\left(K_m - K'_w\right)} \right). \tag{A3}$$

Here K_m and K_f are the mineral and frame bulk moduli, n is the fractional porosity, and the bulk modulus of the pore water (K_w) is modified by the addition of gas (K'_w), introducing a compressible pore fluid:

$$K'_w = \frac{K_w K_g}{n'_g K_g + \left(1 - n'_g\right) K_g}. \tag{A4}$$

In case of adiabatic compression, the bulk modulus of the gas is $K_g = \gamma P_0$, where γ is the ratio of specific heats of gas and P_0 is the ambient hydrostatic pressure. The fraction of sediment pore space occupied by gas (n'_g) is the gas volume (n_g) divided by the fractional porosity (n):

$$n'_g = \frac{n_g}{n}. \tag{A5}$$

Acknowledgments
We wish to thank Niklas Allroggen and Marius Becker for their help with Matlab and Sabine Flury for useful comments on an early draft of the manuscript. We would like to thank the editor and two anonymous reviewers for their helpful and constructive comments that greatly contributed to improving the final version of the manuscript. This research was part of the Baltic Gas project and received the funding from the European Community's Seventh Framework Programme (FP/2007-2013) under grant agreement 217246 made with the joint Baltic Sea research and development program BONUS. The educational user-license grant of IHS Global Inc. and the support of GEDCO allowed us to use the softwares The Kingdom Suite and VISTA 2D/3D Seismic Data Processing.

References

Abegg, F., and A. L. Anderson (1997), The acoustic turbid layer in muddy sediments of Eckernförde Bay, Western Baltic: Methane concentration, saturation and bubble characteristics, *Mar. Geol.*, *137*, 137–147.

Albert, D. B., C. S. Martens, and M. J. Alperin (1998), Biogeochemical processes controlling methane in gassy coastal sediments—Part 2: Groundwater flow control of acoustic turbidity in Eckernförde Bay sediments, *Cont. Shelf Res.*, *18*, 1771–1793.

Algar, C. K., B. P. Boudreau, and M. A. Barry (2011), Initial rise of bubble in cohesive sediments by a process of viscoelastic fracture, *J. Geophys. Res.*, *116*, B04207, doi:10.1029/2010JB008133.

Anderson, A. L., and L. D. Hampton (1980a), Acoustics of gas-bearing sediments. I. Background, *J. Acoust. Soc. Am.*, *67*, 1865–1889.

Anderson, A. L., and L. D. Hampton (1980b), Acoustics of gas-bearing sediments. II. Measurements and models, *J. Acoust. Soc. Am.*, *67*, 1890–1903.
Anderson, A. L., F. Abegg, J. A. Hawkins, M. E. Duncan, and E. P. Lyons (1998), Bubble populations and acoustic interaction with the gassy floor of Eckernförde Bay, *Cont. Shelf Res.*, *18*, 1807–1839.
Andrén, E., T. Andrén, and G. Sohlenius (2000), The Holocene history of the southwestern Baltic Sea as reflected in a sediment core from the Bornholm Basin, *Boreas*, *19*, 233–250.
Andrén, T., S. Björk, E. Andrén, D. Conley, L. Zillén, and J. Anjar (2011), Development of the Baltic Sea Basin during the last 130 ka, in *The Baltic Sea Basin, Central and Eastern European Development Studies (CEEDES)*, edited by J. Harff et al., pp. 75–97, Springer, Berlin Heidelberg.
Best, A. I., M. D. J. Tuffin, J. K. Dix, and J. M. Bull (2004), Tidal height and frequency dependence of acoustic velocity and attenuation in shallow gassy marine sediments, *J. Geophys. Res.*, *109*, B08101, doi:10.1029/2003JB002748.
Björk, S. (1995), A review of the history of the Baltic Sea, 13.0–8.0 ka BP, *Quat. Int.*, *27*, 19–40.
Boetius, A., K. Ravenschlag, C. J. Schubert, D. Rickert, F. Widdel, A. Gieseke, R. Amann, B. B. Jorgensen, U. Witte, and U. Pfannkuche (2000), A marine microbial consortium apparently mediating anaerobic oxidation of methane, *Nature*, *407*, 623–626.
Boudreau, B. P. (2012), The physics of bubbles in surficial, soft, cohesive sediments, *Mar. Pet. Geol.*, *38*, 1–18.
Boudreau, B. P., C. Algar, B. D Johnson, I. Croudace, A. Reed, Y. Furukawa, K. M. Dorgan, P. A. Jumars, A. S. Grader, and B. S. Gardiner (2005), Bubble growth and rise in soft sediments, *Geology*, *33*, 517–520.
Dickens, G. R. (2011), Down the rabbit hole: Toward appropriate discussion of methane release from gas hydrate systems during the Paleocene-Eocene thermal maximum and other past hyperthermal events, *Clim. Past*, *7*, 831–846.
Dix, C. H. (1955), Seismic velocities from surface measurements, *Geophysics*, *20*, 68–86.
Dvorkin, J., and A. Nur (1998), Acoustic signatures of patchy saturation, *Int. J. Solids Struct.*, *35*, 4803–4810.
Ecker, C., J. Dvorkin, and A. M. Nur (2000), Estimating the amount of gas-hydrate and free gas from marine data, *Geophysics*, *65*, 565–573.
Fleischer, P., T. H. Orsi, M. D. Richardson, and A. L. Anderson (2011), Distribution of free gas in marine sediments: A global overview, *Geo-Mar. Lett.*, *21*, 103–122.
Fossing, H. (2005a), Biogeochemistry and physical properties in core GT04-314G, PANGAEA, doi:10.1594/PANGAEA.327657.
Fossing, H. (2005b), Biogeochemistry and physical properties in core GT04-276MUC, tube B, doi:10.1594/PANGAEA.327762.
Fu, S. S., R. H. Wilkens, and L. N. Frazer (1996), In situ velocity profiles in gassy sediments: Kiel Bay, *Geo-Mar. Lett.*, *16*, 249–253.
Gardner, T. N. (2000), An acoustic study of soils that model seabed sediments containing gas bubbles, *J. Acoust. Soc. Am.*, *107*, 163–176.
Gardner, T. N., and G. C. Sills (2001), An examination of the parameters that govern the acoustic behavior of sea bed sediments containing gas bubbles, *J. Acoust. Soc. Am.*, *110*, 1878–1889.
Gassmann, F. (1951), Über die Elastizität poröser Medien, *Vierteljahrschrift der Naturforschenden Gesellscahft in Zürich*, *96*, 1–23.
Graversen, O. (2009), Structural analysis of superposed fault systems of the Bornholm horst block, Tornquist Zone, Denmark, *Bull. Geol. Soc. Den.*, *57*, 25–49.
Hajnal, Z., and I. T. Sereda (1981), Maximum uncertainty of interval velocity estimates, *Geopysics*, *46*, 1543–1547.
Jensen, J. B., and O. Bennike (2009), Geological setting as background for methane distribution in Holocene mud deposits, Aarhus Bay, Denmark, *Cont. Shelf Res.*, *29*, 755–784.
Judd, A. G. (2004), Natural seabed gas seeps as sources of atmospheric methane, *Environ. Geol.*, *46*, 988–996.
Judd, A. G., and M. Hovland (1992), The evidence of shallow gas in marine sediments, *Cont. Shelf Res.*, *12*, 717–725.
Kögler, F.-C., and B. Larsen (1979), The West Bornholm basin in the Baltic Sea: Geological structure and Quaternary sediments, *Boreas*, *8*, 1–22.
Laier, T., and J. B. Jensen (2007), Shallow gas depth-contour map of the Skagerrak-western Baltic Sea region, *Geo-Mar. Lett.*, *27*, 127–141.
Lee, M. W., D. R. Hutchinson, W. P. Dillon, J. J. Miller, W. F. Agena, and B. A. Swift (1993), Method of estimating the amount of in situ gas hydrates in deep marine sediments, *Mar. Pet. Geol.*, *10*, 493–506.
Lee, M. W., D. R. Hutchinson, T. S. Collett, and W. P. Dillon (1996), Seismic velocities for hydrate-bearing sediments using weighted equation, *J. Geophys. Res.*, *101*, 20,347–20,358.
Liu, X., and P. B. Flemings (2006), Passing gas through the hydrate stability zone at southern Hydrate Ridge, offshore Oregon, *Earth Planet. Sc. Lett.*, *241*, 211–226.
Majewski, P., and Z. Klusek (2011), Expressions of shallow gas in the Gdansk Basin, *Zeszyty Naukowe AMW*, *187*, 61–71.
Martens, C. S., D. B. Albert, and M. J. Alperin (1998), Biogeochemical processes controlling methane in gassy coastal sediments—Part 1. A model coupling organic natter flux to gas production, oxidation and transport, *Cont. Shelf Res.*, *18*, 1741–1770.
Mathys, M., O. Thiessen, F. Theilen, and M. Schmidt (2005), Seismic characterization of gas-rich near surface sediments in the Arkona Basin, Baltic Sea, *Mar. Geophys. Res.*, *26*, 207–224.
Milucka, J., T. G. Ferdelman, L. Polerecky, D. Franzke, G. Wegener, M. Schmid, I. Lieberwirth, M. Wagner, F. Widdel, and M. M. M. Kuypers (2012), Zero-valent sulphur is a key intermediate in marine methane oxidation, *Nature*, *491*, 541–546.
Mogollón, J. M., I. L'Heureux, A. W. Dale, and P. Regnier (2009), Methane gas-phase dynamics in marine sediments: A model study, *Am. J. Sci.*, *309*, 189–220.
Mogollón, J. M., A. W. Dale, I. L'Heureux, and P. Regnier (2011), Impact of seasonal temperature and pressure changes on methane gas production, dissolution, and transport in unfractured sediments, *J. Geophys. Res.*, *116*, G03031, doi:10.1029/2010JG001592.
Mogollón, J. M., A. W. Dale, H. Fossing, and P. Regnier (2012), Timescales for the development of methanogenesis and free gas layers in recently-deposited sediments of Arkona Basin (Baltic Sea), *Biogeosciences*, *9*, 1915–1933.
Mogollón, J. M., A. W. Dale, J. B. Jensen, M. Schlüter, and P. Regnier (2013), A method for the calculation of anaerobic oxidation of methane rates across regional scales: An example from the Belt Seas and The Sound (North Sea–Baltic Sea transition), *Geo-Mar. Lett.*, *33*, 299–310.
Reeburgh, W. S. (1969), Observations of Gases in Chesapeake Bay Sediments, *Limnol. Oceanogr.*, *14*, 368–375.
Reeburgh, W. S. (2007), Oceanic methane biogeochemistry, *Chem. Rev.*, *107*, 486–513.
Sansone, F. J., and C. S. Martens (1978), Methane oxidation in Cape Lookout Bight, North-Carolina, *Limnol. Oceanogr.*, *23*, 349–355.
Schneider von Deimling, J., W. Weinrebe, Zs. Tóth, H. Fossing, R. Endler, G. Rehder, and V. Spiess (2013), A low frequency multibeam assessment: Spatial mapping of shallow gas by enhanced penetration and angular response anomaly, *Mar. Petrol. Geol.*, *44*, 217–222.
Sviridov, N. I., J. V. Frandsen, T. H. Larsen, V. Friis-Christensen, K. E. Madsen, and H. Lykke-Andersen (1995), The geology of Bornholm Basin, *Aarhus Geosci.*, *5*, 15–35.
Thießen, O., M. Schmidt, F. Theilen, M. Schmitt, and G. Klein (2006), Methane formation and distribution of acoustic turbidity in organic-rich surface sediments in the Arkona Basin, Baltic Sea, *Cont. Shelf Res.*, *26*, 2469–2483.

Tréhu, A. M., P. B. Flemings, N. L. Bangs, J. Chevallier, E. Grá cia, J. E. Johnson, C.-S. Liu, X. Liu, M. Riedel, and M. E. Torres (2004), Feeding methane vents and gas hydrate deposits at south Hydrate Ridge, *Geophys. Res. Lett.*, *31*, L23310, doi:10.1029/2004GL021286.

Vejbæk, O. V. (1985), *Seismic Stratigraphy and Tectonics of Sedimentary Basins Around Bornholm, Southern Baltic, Danmarks Geologiske Undersøgelse Serie A*, vol. 8, Komm. C. A. Reitzel, Copenhagen.

Wheeler, S. J. (1988), A conceptual model for soils containing large gas bubbles, *Géotechnique*, *38*, 389–397.

Wheeler, S. J., and T. N. Gardner (1989), The elastic moduli of soils containing large gas bubbles, *Géotechnique*, *39*, 333–342.

Wilkens, R. H., and M. D. Richardson (1998), The influence of gas bubbles on sediment acoustic properties: In situ, laboratory, and theoretical results from Eckernförde Bay, Baltic Sea, *Cont. Shelf Res.*, *18*, 1859–1892.

Wood, W. T., P. L. Stoffa, and T. H. Shipley (1994), Quantitative detection of methane hydrate through high-resolution seismic velocity analysis, *J. Geophys. Res.*, *99*, 9681–9695.

Yilmaz, Ö. (2001), *Seismic Data Analysis: Processing, Inversion, and Interpretation of Seismic Data*, DVD ed., Society of Exploration Geophysicists (SEG), Tulsa, Okla.